

Wavelength-tunable, passively mode-locked fiber laser based on graphene and chirped fiber Bragg grating

Xiaoying He,^{1,2} Zhi-bo Liu,^{1,3} and D. N. Wang^{1,*}

¹Department of Electrical Engineering, The Hong Kong Polytechnic University, Hung Hom, Kowloon, China

²Department of Optical Science and Engineering, Fudan University, Shanghai 200433, China

³Key Laboratory of Weak Light Nonlinear Photonics, Ministry of Education, Teda Applied Physics School, Nankai University, Tianjin 300457, China

*Corresponding author: eednwang@polyu.edu.hk

Received March 13, 2012; revised May 25, 2012; accepted May 27, 2012;
posted May 29, 2012 (Doc. ID 164678); published June 13, 2012

We demonstrate a wavelength-tunable, passively mode-locked erbium-doped fiber laser based on graphene and chirped fiber Bragg grating. The saturable absorber used to enable passive mode-locking in the fiber laser is a section of microfiber covered by graphene film, which allows light-graphene interaction via the evanescent field of the microfiber. The wavelength of the laser can be continuously tuned by adjusting the chirped fiber Bragg grating, while maintaining mode-locking stability. Such a system has high potential in tuning the mode-locked laser pulses across a wide wavelength range. © 2012 Optical Society of America

OCIS codes: 140.7090, 140.4050.

Passively mode-locked fiber lasers have attracted increased research interests because of their compactness, low cost and widespread applications in optical communications, medicine, and materials processing [1–4]. Currently, the majority of passively mode-locked fiber lasers employ a saturable absorber (SA), including a semiconductor saturable absorber mirror (SESAM) and single-wall carbon nanotubes (SWCNTs), to convert the continuous laser light into optical pulse trains [4–8]. It is desirable to have an ultrafast and broadband SA, as the central wavelength of the ultrafast pulses can be tuned across a number of available transmission channels.

Graphene appears to be a promising candidate for the SA because of the gapless linear dispersion of Dirac electrons and Pauli blocking, which enable ultrafast and broadband saturable absorption prosperity [9–11]. Moreover, the graphene-based SA is superior to SESAM and SWCNTs as it requires no bandgap or diameter control to achieve broadband saturable absorption.

Various approaches have been exploited to enable wavelength-tunable operation in passively mode-locked fiber lasers, such as to use a tunable bandpass filter [12,13], an unbalanced Mach–Zehnder interferometer (UMZI) [14], or a Sagnac fiber filter with a thermoelectric cooler (TEC) [15] as the wavelength selective element. However, to maintain the mode-locking stability in the above-mentioned systems, each wavelength tuning step should be followed by polarization controller (PC) adjustment, which is a rather slow process.

In this Letter, we propose and demonstrate a wavelength-tunable, passively mode-locked fiber laser based on graphene-covered-microfiber and chirped fiber Bragg grating (CFBG). The graphene-covered-microfiber plays the role of SA, and is fabricated by transferring graphene film onto a microfiber to enable light-graphene interaction along the fiber length. In such a system, once the mode-locking operation is established, no adjustment of PC is needed, even when the peak wavelength of the CFBG is tuned.

The passively mode-locked erbium-doped fiber (EDF) laser with a ring cavity configuration is shown in Fig. 1. A

1.5 m high concentration EDF (OFS EDF-80) is used as the gain medium, pumped by a 1480 nm high power laser diode via a 980 nm/1550 nm wavelength division multiplexer (WDM) coupler. The function of the isolator is to further enhance the unidirectional pulse propagation in the fiber laser system. An optical circulator (OC) is used to direct the light into the CFBG, which is mounted on the top surface of a triangular cantilever beam. By pressing the vertex of the cantilever beam, the wavelength of the output pulses can be changed. The PC is used to control the polarization state of the light launched into the graphene-based SA. The mode-locked pulses generated are directed out by a 90:10 optical coupler. One of the main factors to maintain the mode-locked fiber laser stability is the group velocity dispersion (GVD). The GVD of the EDF used in the system is ~ -46.25 ps²/nm²/km, at the wavelength of 1560 nm. The microfiber is 4 cm in length and has a small anomalous dispersion of ~ 6 ps²/nm²/km. The total laser cavity length is 14.96 m, and the round-trip dispersion of the whole cavity is ~ 0.172 ps²/nm. The laser output spectrum is recorded by an optical spectrum analyzer (ANDO AQ6319) with a 0.01 nm resolution. The radio frequency (RF) spectrum of the passively mode-locked fiber laser is measured by use of a high speed photo-detector (New-focus 1414, 25 GHz) connected to a real-time spectrum analyzer (Tektronix RSA 3303A, 3 GHz). The pulse is monitored by a second harmonic generation (SHG) autocorrelator (FEMTOCHROME FR-103XL, resolution <5 fs) together with a high speed photo-detector connected to an oscilloscope (Tektronix, TPS 2024).

To fabricate the graphene-based SA, the monolayer graphene film is directly synthesized by the chemical vapor deposition (CVD) method on polycrystalline Cu substrate [16]. The polymer clad resin (EfiRON, PC-373) is adhered to the graphene films on a Cu substrate and is then cured by ultraviolet light. After 24 hours, the supporting/graphene/metal layers are soaked with FeCl₃ solution to remove the metal layers. Finally, the resulting polymer-supported monolayer graphene film can be transferred onto the microfiber surface and used as

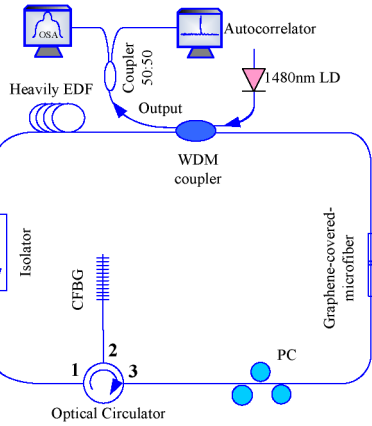


Fig. 1. (Color online) Experimental setup of the wavelength-tunable, passively mode-locked fiber laser. LD, laser diodes; WDM, wavelength division multiplexer; EDF, erbium-doped fiber; CFBG, chirped fiber Bragg grating; PC, polarization controller.

the graphene-based SA in the fiber laser system. The microfiber with a diameter of $\sim 12 \mu\text{m}$ is fabricated by use of the flame brushing method from the single-mode fiber [17,18]. The low loss and large evanescent field [19] of the microfiber enable it to be easily coupled with other nanosized optical materials such as graphene. Compared to the other methods of fabricating graphene-based SA [9–11], our approach is easy to do and results in a large light-graphene interaction length. Moreover, by

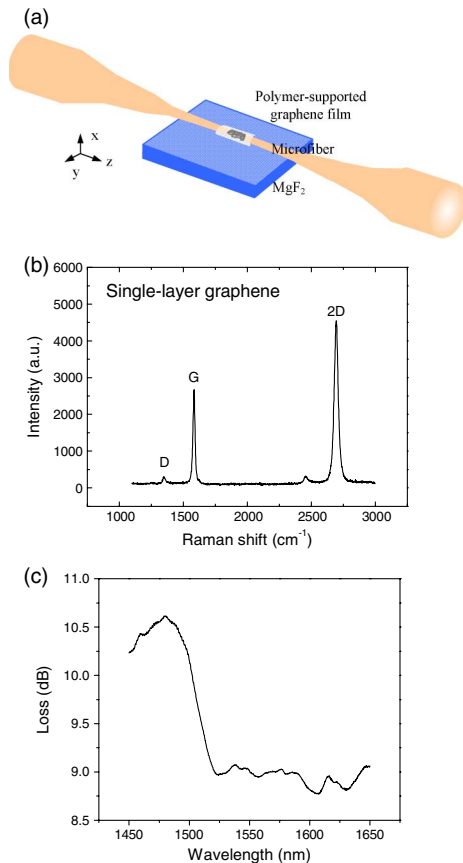


Fig. 2. (Color online) (a) Schematic structure of the graphene-based SA. (b) Raman spectra of monolayer graphene. (c) Insertion loss of the graphene-based SA.

applying pressure on an aluminum sheet placed on top of the graphene sheet, the microfiber and graphene sheet can be closely touched. The schematic structure of the graphene-based SA is shown in Fig. 2(a). A typical Raman spectrum of monolayer graphene measured by a 512 nm laser source and a $50\times$ objective lens is displayed in Fig. 2(b). It can be observed from this figure that three peaks, D, G, and two-dimensional (2D) bands, are situated at ~ 1345 , 1573 , and 2688 cm^{-1} , respectively. For the monolayer graphene, the Raman 2D band is much stronger than G band with a 2D/G ratio of 1.76. The weak D band indicates a low density of defects and high crystallinity of the CVD-grown graphene. The typical modulation depth of graphene SA is $\sim 12.88\%$, the non-aturable loss is $\sim 7.56 \text{ dBm}$, and the saturation intensity is $\sim 48 \text{ mW/cm}^2$. By use of a broadband continuous wave (CW) light source, the measured insertion loss of the graphene-based SA is varied between ~ 10.5 and 9 dB , within the wavelength range between 1450 and 1650 nm , as indicated in Fig. 2(c). The variation in insertion losses of SA is due to the pressure applied on it as the large deformation of the microfiber leads to the large scattering and bending losses, which are wavelength dependent. Thus the insertion loss of SA is also wavelength-dependent.

As demonstrated in Fig. 3(a), the laser output pulse train has a period of $\sim 74.8 \text{ ns}$, which matches well with the cavity round-trip time and verifies that the laser is indeed in passive mode-locking scheme. Figure 3(b) shows the RF measurement results of the laser output. The basic repetition rate is $\sim 27 \text{ MHz}$, corresponding

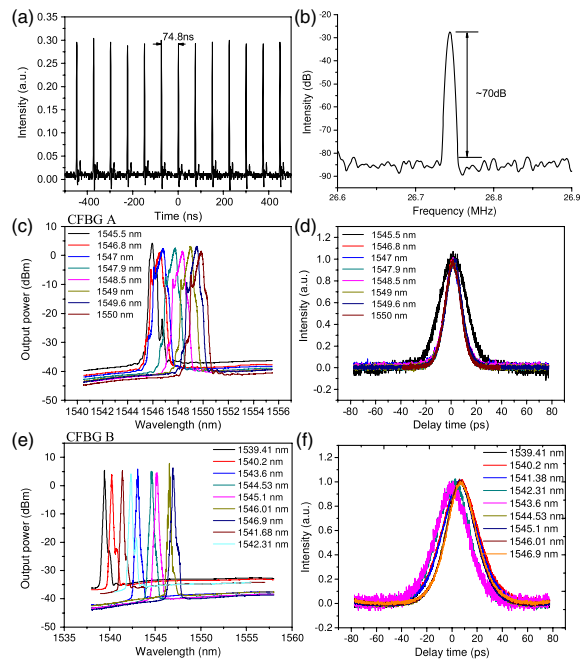


Fig. 3. (Color online) Characteristics of the wavelength-tunable passively mode-locked fiber laser. (a) Output pulse train; (b) RF spectrum, measured around the fundamental repetition rate $\sim 26.7 \text{ MHz}$ over 1 MHz with 10 Hz resolution; (c) output spectra under CFBG A; (d) autocorrelation traces at different wavelengths under CFBG A; (e) output spectra under CFBG B; (f) autocorrelation traces at different wavelengths under CFBG B.

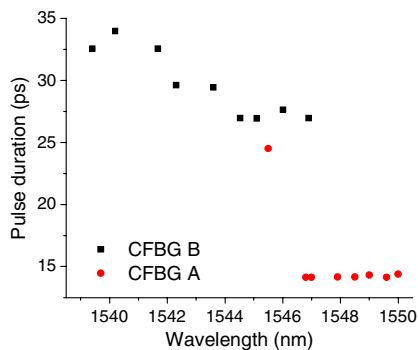


Fig. 4. (Color online) Output pulse duration versus wavelength.

to the ~ 74.8 ns round-trip time obtained in Fig. 3(a). The signal-to-noise ratio of >70 dB is observed, showing the good mode-locking stability of the fiber laser system [20]. In the experiment, two CFBGs: CFBG A and CFBG B, are used separately, with the central wavelength of ~ 1547 and 1541.2 nm, reflectivity of ~ 16 and ~ 10 dB, and 3 dB bandwidth of 1.6 and 1.05 nm, respectively. By tuning CFBG A, the output wavelength can be changed from 1545.5 to 1550 nm, as revealed in Fig. 3(c). The typical soliton sidebands can be observed, due to the periodic intracavity perturbations. The AC traces of the laser pulses obtained are shown in Fig. 3(d), with pulse durations of ~ 14 ps. By replacing CFBG A with CFBG B, the output wavelength can be tuned from 1539.4 to 1546 nm, as depicted in Fig. 3(e). The corresponding AC traces shown in Fig. 3(f) have the pulse durations of ~ 26 ps. The spectra shown in Figs. 3(c) and 3(e) have the 3 dB bandwidths of 0.4 and 0.2 nm, respectively, limited by the bandwidth of the CFBG reflection spectrum. The laser pulse duration corresponding to different operating wavelength is shown in Fig. 4, which can be decreased from 34 to 27 ps and from 24 to 14 ps by adjusting CFBG B and CFBG A, respectively. In the passively mode-locked fiber laser, the pulse duration mainly depends on the dispersion of the system and the chirp introduced by the CFBG. The values of dispersion and chirp are quite different when the output wavelength of the fiber laser operates at 1545.5 and 1547 nm, respectively. Thus, there is a big leap in pulse period between 1545.5 and 1547 nm, as shown in Fig. 4. The fact that the shorter wavelengths have longer pulse duration than that of the longer wavelengths is probably due to the higher insertion loss of the CFBG at the shorter wavelengths.

In conclusion, a wavelength-tunable, passively mode-locked fiber laser based on graphene-covered-microfiber and a CFBG has been demonstrated. The method of integrating graphene film onto optical microfiber is simple and effective. The wavelength tuning of the laser pulses

can be conveniently implemented by adjusting the CFBG. The system has high potential in supporting wide range mode-locked laser wavelength tuning.

This work was supported by the Hong Kong SAR government through a general research fund (GRF) grant PolyU 5298/10E, and the Fundamental Research Funds for the Central University GKH1232000/007. The authors would like to thank Mr. Hu Tianyi for assistance in the experiment and Prof. Mark MacAlpine for language polishing.

Reference

1. V. S. Letokhov, *Nature* **316**, 325 (1985).
2. M. E. Ferman, A. Galvanauska, and G. Sucha *Ultrafast Lasers: Technology and Application* (Dekker, 2003).
3. H. Endert, A. Galvanauskas, G. Sucha, R. Patel, and M. Stock, *RIKEN Rev.* **43**, 23 (2002).
4. U. Keller, *Nature* **424**, 831 (2003).
5. O. Okhotnikov, A. Grudinin, and M. Pessa, *New J. Phys.* **6**, 177 (2004).
6. T. Hasan, Z. Sun, F. Wang, F. Bonaccorso, P. H. Tan, A. G. Rozhin, and A. C. Ferrari, *Adv. Mater.* **21**, 3874 (2009).
7. F. Wang, A. G. Rozhin, V. Scardaci, Z. Sun, F. Hennrich, I. H. White, W. I. Milne, and A. C. Ferrari, *Nat. Nanotechnol.* **3**, 738 (2008).
8. S. Y. Set, H. Yaguchi, Y. Tanaka, and M. Jablonski, *IEEE J. Sel. Top. Quantum Electron.* **10**, 137 (2004).
9. Z. Sun, T. Hasan, F. Torrisi, D. Popa, G. Privitera, F. Wang, F. Bonaccorso, D. M. Basko, and A. C. Ferrari, *ACS Nano* **4**, 803 (2009).
10. Q. Bao, H. Zhang, Y. Wang, Z. Ni, Y. Yan, Z. X. Shen, K. P. Loh, and D. Y. Tang, *Adv. Funct. Mater.* **19**, 3077 (2009).
11. Q. Bao, H. Zhang, J. Yang, S. Wang, D. Y. Tang, R. Jose, S. Ramakrishna, C. T. Lim, and K. P. Loh, *Adv. Funct. Mater.* **20**, 782 (2010).
12. Z. Sun, D. Popa, T. Hasan, F. Torrisi, F. Wang, E. J. R. Kelleher, J. C. Travers, V. Nicolosi, and A. C. Ferrari, *Nano Res.* **3**, 653 (2010).
13. H. Sotobayashi, J. T. Gopinath, E. M. Koontz, L. A. Kolodziejski, and E. P. Ippen, *Opt. Commun.* **237**, 399 (2004).
14. S. M. Zhang, Q. S. Meng, and G. Z. Zhao, *Eur. Phys. J. D* **60**, 383 (2010).
15. B. Ibarra-Escamilla, O. Pottiez, J. W. Haus, E. A. Kuzin, M. Bello-Jimenez, and A. Flores-Rosas, *J. Eur. Opt. Soc.* **3**, 08036 (2008).
16. S. Chen, W. Cai, R. D. Piner, J. W. Suk, Y. Wu, Y. Ren, J. Kang, and R. S. Ruoff, *Nano Lett.* **11**, 3519 (2011).
17. X. Fang, C. R. Liao, and D. N. Wang, *Opt. Lett.* **35**, 1007 (2010).
18. Y. Jung, G. Brambilla, K. Oh, and D. J. Richardson, *Opt. Lett.* **35**, 378 (2010).
19. L. Tong, J. Lou, and E. Mazur, *Opt. Mater. Express* **12**, 1025 (2004).
20. D. von der Linde, *Appl. Phys. B* **39**, 201 (1986).